

# Confinement and the photon propagator in 3D compact QED: a lattice study in Landau gauge at zero and finite temperature

M. N. Chernodub

*Institute of Theoretical and Experimental Physics,  
B. Chermushkinskaja 25, Moscow, 117259, Russia and*

*Institute for Theoretical Physics, Kanazawa University, Kanazawa 920-1192, Japan*

E.-M. Ilgenfritz

*Research Center for Nuclear Physics, Osaka University, Osaka 567-0047, Japan*

A. Schiller

*Institut für Theoretische Physik and NTZ,  
Universität Leipzig, D-04109 Leipzig, Germany*

(Dated: February 8, 2020)

On the lattice we study the gauge boson propagator of three dimensional compact QED in Landau gauge at zero and non-zero temperature. The non-perturbative effects are taken into account by the generation of a mass, by an anomalous dimension and by the photon wave function renormalization. All these effects can be attributed to the monopoles: they are absent in the propagator of the singularity-free part of the gauge field. We assess carefully the Gribov copy problem for the propagator and the parameters emerging from the fits.

PACS numbers: 11.15.Ha, 11.10.Wx, 12.38.Gc

## I. INTRODUCTION

Three-dimensional compact electrodynamics (cQED<sub>3</sub>) has two essential features in common with QCD, confinement [1] and chiral symmetry breaking [2]. Although the physics behind it might be very different, monopole dynamics in three and in four dimensions, it is amusing to study certain non-perturbative aspects within a lower-dimensional model like cQED<sub>3</sub>. Apart from its role as a toy model for QCD, the non-perturbative properties of cQED<sub>3</sub> deserve interest by themselves because this model was shown to describe some features of Josephson junctions [3] and high- $T_c$  superconductors [4]. cQED<sub>3</sub> has been the first example, in space-time dimensions greater than two where it becomes a non-trivial problem, in which confinement of electrically charged particles was understood analytically [1]. It is the result of the dynamics of monopoles which emerge due to the compactness of the gauge field. Other common features of cQED<sub>3</sub> and QCD are the existence of a mass gap and of a confinement-deconfinement phase transition at some non-zero temperature.

In two recent papers we have demonstrated how the deconfinement phase transition, occurring under the influence of compactification of one dimension, in  $2 + 1$  dimensions, finds its explanation from the monopole point of view [5] and why the deconfinement phase transition is independent on the strength of the external fields [6].

In a recent letter [7] we answered the question what effect the confinement property has on the gauge boson propagator in this theory and what of the propagator is changing at the deconfinement temperature. The effects are twofold: first, an anomalous dimension appears which modifies the momentum dependence, and second, a mass is generated which can be well understood in terms of Polyakov's theory [1]. In Ref. [7] we also have used the unique possibility in lattice simulations to remove the monopole degrees of freedom from the quantum gauge field in order to show that all nontrivial effects reside exclusively in the singular fields of the monopoles.

Note that a non-trivial anomalous dimension of the gauge boson propagator may also appear due to dynamical matter fields [8]. The sign (in our notations) of the anomalous dimension induced in this way is different and this leads to the binding of the monopoles into dipole pairs and, consequently, to the disappearance of the confinement at certain distances between the test particles. This picture was confirmed for the compact model in the presence of the dynamical matter fields [9].

In the present paper we want to extend the analysis of Ref. [7] in various respects. Since the propagator is studied in the Landau gauge, first of all we have investigated more carefully the quality of the gauge fixing and the importance of the Gribov copy problem, first on the propagator itself and then on the parameters which finally describe the functional form of the propagator.

In a second direction, we investigate the potential influence that different definitions of the gauge potential  $A_\mu$  in terms of the lattice link fields might have on the resulting propagator. One of the choices is strongly recommended by the explicit gauge invariance (transversality) of the emerging propagator. However, also in the case when the longitudinal part does not vanish by construction, proper selection of the transversal component leads to almost the same fit parameters. The coincidence becomes obviously better at larger  $\beta$ .

Going over from zero to finite temperature, it is important to realize that more structure functions are necessary to describe the finite-temperature case. One of them, the deconfinement-sensitive  $D_L$ , has been studied already in Ref. [7], while the other,  $D_T$ , has been found to be extremely sensitive to the Gribov problem. Only exerting extreme care one can expose the change going on at the deconfinement transition.

The paper is organized as follows. In section II we define the lattice model and the tensorial structure of the propagators, at  $T = 0$  and for  $T \neq 0$ . Section III contains a discussion of the minimal Landau gauge which points out the topological aspects related to the gauge fixing, in particular the condition of having a minimal total length of Dirac strings. In section IV we report on the numerical algorithms for updating and gauge fixing which we have used in our investigation. The following section V is devoted to an outline of the results for  $T = 0$ . Section VI describes the particular requirements of gauge fixing in the  $T \neq 0$  case and contains our results for the propagators  $D_L$  and  $D_T$ . Some conclusions are formulated in section VII.

## II. THE 3D COMPACT U(1) MODEL AND THE PHOTON PROPAGATOR

For the compact U(1) model we chose the Wilson single-plaquette action:

$$S[\theta_l] = \beta \sum_p (1 - \cos \theta_p), \quad (1)$$

where  $\theta_p$  is the  $U(1)$  field strength tensor represented by the plaquette curl of the compact link field  $\theta_l$ . The lattice is three-dimensional, and the basic degrees of freedom are the links  $U_l = \exp(i \theta_l)$ . The measure of the link angles is flat over the interval  $-\pi < \theta \leq \pi$ . The lattice coupling constant  $\beta$  is related to the lattice spacing  $a$  and the continuum coupling constant  $g_3$  of the 3D theory,

$$\beta = 1/(a g_3^2) . \quad (2)$$

Note that in three dimensional gauge theory the coupling constant  $g_3$  has dimension mass<sup>1/2</sup>. Zero physical temperature is represented by symmetric lattices,  $L_t = L_s$ .<sup>1</sup> The lattice corresponding to finite temperature is asymmetric,  $L_s^2 \times L_t$ ,  $L_t \ll L_s$ . In the limit  $L_s \rightarrow \infty$ , the temporal extension of the lattice is related to the physical temperature,  $L_t = 1/(Ta)$ . Using (2) the temperature is given in units of  $g_3^2$  in terms of the lattice parameters as follows:

$$\frac{T}{g_3^2} = \frac{\beta}{L_t} . \quad (3)$$

Our simulations for zero temperature have been performed mainly on a  $32^3$  lattice, those at finite temperature on a  $32^2 \times 8$  lattice.

The final discussion of the photon propagator will be given in lattice momentum space. Being always defined in a specified gauge, the propagator is written in terms of the Fourier transformed gauge potential,

$$\tilde{A}_{\vec{k},\mu} = \frac{1}{\sqrt{L_1 L_2 L_3}} \sum_{\vec{n}} \exp\left(2\pi i \sum_{\nu=1}^3 \frac{k_\nu (n_\nu + \frac{1}{2}\delta_{\nu\mu})}{L_\nu}\right) A_{\vec{n}+\frac{1}{2}\vec{\mu},\mu} , \quad (4)$$

which is a sum over a certain discrete set of points  $\vec{x} = \vec{n} + \frac{1}{2}\vec{\mu}$  forming the support of  $A_{\vec{x},\mu}$  on the lattice. These are the midpoints of the links in  $\mu$  direction while  $\vec{n}$  denotes the lattice sites (nodes) with integer Cartesian coordinates. The propagator is the gauge-fixed ensemble average of the following bilinear in  $\tilde{A}$ ,

$$D_{\mu\nu}(\vec{p}) = \langle \tilde{A}_{\vec{k},\mu} \tilde{A}_{-\vec{k},\nu} \rangle . \quad (5)$$

Two identifications of  $A_{\vec{x},\mu}$  have been adopted in the literature and will be compared in our paper: the *angle*-definition

$$A_{\vec{n}+\frac{1}{2}\vec{\mu},\mu} = \theta_{\vec{n},\mu}/(g a) = \log(U_{\vec{n},\mu})/(i g a) \quad (6)$$

and the *sinus*-definition

$$A_{\vec{n}+\frac{1}{2}\vec{\mu},\mu} = \sin(\theta_{\vec{n},\mu})/(g a) = (U_{\vec{n},\mu} - U_{\vec{n},\mu}^*)/(2 i g a) . \quad (7)$$

The corresponding propagators will be denoted as  $D_{\mu\nu}^{ang}$  or  $D_{\mu\nu}^{sin}$ , respectively.

The lattice momenta  $\vec{p}$  on the left hand side of (5) are related to the integer valued Fourier momenta  $\vec{k}$  as follows:

$$p_\mu(k_\mu) = \frac{2}{a} \sin \frac{\pi k_\mu}{L_\mu} , \quad k_\mu = 0, \pm 1, \dots, \pm \frac{L_\mu}{2} . \quad (8)$$

---

<sup>1</sup>  $L_t$  is the extension in the third ( $z$ ) direction.

The lattice equivalent of  $p^2 = \vec{p}^2$  is in  $3D$

$$p^2(\vec{k}) = \frac{4}{a^2} \sum_{\mu=1}^3 \left( \sin \frac{\pi k_{\mu}}{L_{\mu}} \right)^2. \quad (9)$$

At zero temperature, based on Euclidean rotational invariance, the continuum propagator would be expressible by functions of  $p^2$ . The most general tensor structure is then the following one including two scalar functions of  $p^2$ ,

$$D_{\mu\nu}(\vec{p}) = P_{\mu\nu}(\vec{p}) D(p^2) + \frac{p_{\mu}p_{\nu}}{p^2} \frac{F(p^2)}{p^2} \quad (10)$$

with the  $d$ -dimensional (in our case  $d = 3$ ) transverse projection operator

$$P_{\mu\nu}(\vec{p}) = \delta_{\mu\nu} - \frac{p_{\mu}p_{\nu}}{p^2}. \quad (11)$$

The projector has the properties

$$P_{\mu\alpha}(\vec{p}) P_{\alpha\nu}(\vec{p}) = P_{\mu\nu}(\vec{p}), \quad P_{\mu\mu}(\vec{p}) = d - 1. \quad (12)$$

The two structure functions  $D(p^2)$  and  $F(p^2)$  can be extracted by projection, on the lattice from  $D_{\mu\nu}(\vec{p})$  according to (5), as

$$F(p^2) = \sum_{\mu,\nu=1}^3 p_{\mu} D_{\mu\nu}(\vec{p}) p_{\nu} \quad (13)$$

and

$$p^2 D(p^2) = \frac{1}{d-1} P_{\mu\nu}(\vec{p}) D_{\mu\nu}(\vec{p}). \quad (14)$$

They are found, in the best case, only approximately rotationally invariant, *i.e.* individual momenta  $\vec{p}$  might slightly differ in the function values  $D$  or  $F$  they provide, even if they have the same  $p^2$ . Nearby, in  $p^2$  dense data points might scatter rather than forming a smooth function of  $p^2$ .

In practice, using these definitions, we extract at first the function  $F(p^2)$ , in the  $d = 3$  case through

$$F(p^2) = p_1^2 D_{11}(\vec{p}) + p_2^2 D_{22}(\vec{p}) + p_3^2 D_{33}(\vec{p}) + 2p_1 p_2 \text{Re} D_{12}(\vec{p}) + 2p_1 p_3 \text{Re} D_{13}(\vec{p}) + 2p_2 p_3 \text{Re} D_{23}(\vec{p}). \quad (15)$$

The imaginary parts of non-diagonal  $D_{\mu\nu}$  cancel in the sum and have been omitted. Then, the function  $D(p^2)$  is obtained through

$$D(p^2) = \frac{1}{d-1} [(D_{11}(\vec{p}) + D_{22}(\vec{p}) + D_{33}(\vec{p})) - F(p^2)/p^2]. \quad (16)$$

If the Landau gauge would be exactly fulfilled, one would expect that  $F(p^2) \equiv 0$ . On the lattice, in the case of the *sinus*-definition for  $A_{\vec{x},\mu}$ , this is actually the case as soon as

one of the Gribov copies is reached, with an accuracy which directly reflects the stopping precision of the gauge fixing procedure (as will be discussed below). In this case, a simplified definition in terms of the diagonal components  $D_{\mu\mu}(\vec{p})$  would be appropriate. In case of the *angle*-definition the structure function  $F(p^2)$  does not vanish, therefore all components of  $D_{\mu\nu}(\vec{p})$  contribute to  $D(p^2)$ .

For the finite temperature case, the propagator lacks  $O(3)$  rotational symmetry. Now we have to consider two scalar functions,  $D_T$  and  $D_L$  instead of  $D$ , each multiplying the  $(d-1)$ -dimensional transverse projection operator  $P^T$  and the  $(d-1)$ -dimensional longitudinal projection operator  $P^L$ , respectively. The scalar functions  $D_T$ ,  $D_L$  and  $F$  depend now separately on the length of the space-like part of  $\vec{p}$  with  $i = 1, \dots, d-1$ ,

$$\mathbf{p}^2 = p_1^2 + \dots + p_{d-1}^2, \quad |\mathbf{p}| = \sqrt{\mathbf{p}^2}, \quad (17)$$

and the ‘‘temporal’’ momentum  $p_d$ :

$$D_{\mu\nu}(\vec{p}) = P_{\mu\nu}^T(\vec{p})D_T(|\mathbf{p}|, p_d) + P_{\mu\nu}^L(\vec{p})D_L(|\mathbf{p}|, p_d) + \frac{p_\mu p_\nu}{p^2} \frac{F(|\mathbf{p}|, p_d)}{p^2}. \quad (18)$$

The two projection operators are defined as follows ( $i, j = 1, \dots, d-1$ ): a transversal one,

$$P_{ij}^T(\vec{p}) = \delta_{ij} - \frac{p_i p_j}{\mathbf{p}^2}, \quad P_{dd}^T(\vec{p}) = P_{di}^T(\vec{p}) = P_{id}^T(\vec{p}) = 0, \quad (19)$$

and a longitudinal one

$$P_{\mu\nu}^L(\vec{p}) = P_{\mu\nu}(\vec{p}) - P_{\mu\nu}^T(\vec{p}). \quad (20)$$

Obviously, these projectors have the properties

$$P_{\mu\alpha}^T(\vec{p}) P_{\alpha\nu}^T(\vec{p}) = P_{\mu\nu}^T(\vec{p}), \quad P_{\mu\mu}^T(\vec{p}) = d-2 \quad (21)$$

$$P_{\mu\alpha}^L(\vec{p}) P_{\alpha\nu}^L(\vec{p}) = P_{\mu\nu}^L(\vec{p}), \quad P_{\mu\mu}^L(\vec{p}) = 1 \quad (22)$$

$$P_{\mu\alpha}^L(\vec{p}) P_{\alpha\nu}^T(\vec{p}) = 0. \quad (23)$$

The scalar functions  $D_T$  and  $D_L$  can be extracted from  $D_{\mu\nu}(\vec{p})$  via

$$P_{\mu\nu}^T(\vec{p}) D_{\mu\nu}(\vec{p}) = (d-2) D_T(|\mathbf{p}|, p_d) \quad (24)$$

$$\begin{aligned} P_{\mu\nu}^L(\vec{p}) D_{\mu\nu}(\vec{p}) &= D_L(|\mathbf{p}|, p_d) \\ &= (d-1) D(|\mathbf{p}|, p_d) - (d-2) D_T(|\mathbf{p}|, p_d). \end{aligned} \quad (25)$$

For  $d=3$  we can write down explicitly the definitions

$$\mathbf{p}^2 D_T(|\mathbf{p}|, p_d) = p_2^2 D_{11}(\vec{p}) + p_1^2 D_{22}(\vec{p}) - 2p_1 p_2 \operatorname{Re} D_{12}(\vec{p}) \quad (26)$$

and

$$\begin{aligned} \mathbf{p}^2 (\mathbf{p}^2 + p_3^2) D_L(|\mathbf{p}|, p_d) &= \mathbf{p}^2 (\mathbf{p}^2 D_{33}(\vec{p}) - 2p_1 p_3 \operatorname{Re} D_{13}(\vec{p}) - 2p_2 p_3 \operatorname{Re} D_{23}(\vec{p})) \\ &\quad + p_3^2 (p_1^2 D_{11}(\vec{p}) + p_2^2 D_{22}(\vec{p}) + 2p_1 p_2 \operatorname{Re} D_{12}(\vec{p})). \end{aligned} \quad (27)$$

In the static limit,  $p_3 = 0$ ,

$$D_L(|\mathbf{p}|, p_3 = 0) \equiv D_{33}(|\mathbf{p}|, p_3 = 0). \quad (28)$$

This propagator for the case of the *angle*-definition and its fit in terms of mass and anomalous dimension as well as the changes at the deconfinement transition have been discussed in Ref. [7].

In the case of  $T = 0$ , the data to be presented below will be averaged over measurements of these quantities obtained for different  $\vec{k} = (k_1, k_2, k_3)$  giving rise to the *same*  $p^2$  according to (9). In the case  $T \neq 0$  we will show data averaged over different  $(k_1, k_2)$  giving rise to the *same*  $\mathbf{p}^2$  according to (17). One should keep in mind that by this “trick” one enforces the rotational invariance “by hand”, and the statistical errors are reduced as compared to measurements for individual  $\vec{k}$ -components of the propagator.

In order to discuss the functional form of the propagator under the aspect of confinement effects, with confinement being induced by the monopole plasma, we will decompose the gauge fields into singular (monopole) and regular (photon) contributions on the level of the link angles,

$$\theta_{\vec{n},\mu} = \theta_{\vec{n},\mu}^{phot} + \theta_{\vec{n},\mu}^{mono}, \quad (29)$$

by a procedure to be described below. After the decomposition (29) of the link angles is done, one may define the corresponding  $A_{\vec{n}+\frac{1}{2}\vec{\mu},\mu}^{phot}$  and  $A_{\vec{n}+\frac{1}{2}\vec{\mu},\mu}^{mono}$  through the *angle*-definition (6) or the *sinus*-definition (7), respectively. Then, by fast Fourier transform, the corresponding  $\tilde{A}_{\vec{k},\mu}^{phot}$  and  $\tilde{A}_{\vec{k},\mu}^{mono}$  are evaluated. For each configuration and a certain set of momenta the bilinears for the photon part  $\tilde{A}_{\vec{k},\mu}^{phot} \tilde{A}_{-\vec{k},\nu}^{phot}$ , the monopole part  $\tilde{A}_{\vec{k},\mu}^{mono} \tilde{A}_{-\vec{k},\nu}^{mono}$  and the mixed bilinear  $\tilde{A}_{\vec{k},\mu}^{phot} \tilde{A}_{-\vec{k},\nu}^{mono}$  are formed. These are the observables which are associated – by averaging over the Monte Carlo ensemble – to the propagators  $D_{\mu\nu}^{phot}(\vec{p})$  (the photon or *regular* propagator),  $D_{\mu\nu}^{mono}(\vec{p})$  (the *singular* propagator) and  $D_{\mu\nu}^{mixed}(\vec{p})$  (the *mixed* propagator). These propagators are considered together with the *full* propagator which uses the original link angles  $\theta_{\vec{n},\mu}$  before the splitting (29) has been performed.

In the  $T = 0$  case, all these functions of  $\vec{p}$  are then mapped by the projections (15,16) to the scalar structure functions  $D^{phot}(p^2)$ ,  $D^{mono}(p^2)$ ,  $D^{mixed}(p^2)$  and  $F^{phot}(p^2)$ ,  $F^{mono}(p^2)$ ,  $F^{mixed}(p^2)$ . In the finite temperature case we proceed analogously.

For the *angle*-definition of the vector potential we stress that the structure functions obviously satisfy exact additivity

$$D(\vec{p}) = D^{phot}(\vec{p}) + D^{mono}(\vec{p}) + 2 D^{mixed}(\vec{p}) \quad (30)$$

$$F(\vec{p}) = F^{phot}(\vec{p}) + F^{mono}(\vec{p}) + 2 F^{mixed}(\vec{p}). \quad (31)$$

### III. MONOPOLES, DIRAC STRINGS AND THE MINIMAL LANDAU GAUGE

In this section we partially follow Ref. [10]. Gauge fixing to the Landau gauge means, for a given configuration  $\theta_l = \theta_{\vec{n},\mu}$ , to find a gauge transformations  $\omega_{\vec{n}}$  such that, for a *gauge functional*

$$\mathcal{F}(\theta) = \sum_l \cos(\theta_l) \quad (32)$$

the transformed gauge functional becomes maximal,

$$\max_{\omega} \mathcal{G}(\theta, \omega), \quad \mathcal{G}(\theta, \omega) = \mathcal{F}(\theta^{(\omega)}). \quad (33)$$

Here  $\theta_l^{(\omega)}$  denotes the gauge transformed gauge field <sup>2</sup>

$$\theta \rightarrow \theta^{(\omega)} = \theta + d\omega_{2\pi} \equiv \theta + d\omega + 2\pi k, \quad k \in \mathbb{Z}, \quad (34)$$

where the integer number  $k = k(\theta, \omega)$  for each link is chosen such that  $\theta^{(\omega)} \in (-\pi, \pi]$ .

Instead of (33), following Ref. [10] we use for the purpose of this section in the following the Villain form of the gauge condition

$$\min_{\omega} \|\theta^{(\omega)}\|^2. \quad (35)$$

The Faddeev–Popov (FP) determinant is introduced by the following decomposition of unity

$$1 = \Delta_{FP}[\theta; \lambda] \int_{-\pi}^{\pi} \mathcal{D}\omega e^{-\lambda \|\theta^{(\omega)}\|^2}, \quad (36)$$

where  $\lambda$  is the gauge fixing parameter. In order to achieve the gauge (35) we have to send  $\lambda$  to infinity. In this case the limits of integration in (36) can be extended to  $\pm\infty$  since the saddle point approximation is exact in the limit  $\lambda \rightarrow \infty$ . Moreover, the integer valued variable  $k$  in (34) becomes effectively independent on  $\theta$  and  $\omega$  since the values of  $k$  for which  $\theta^{(\omega)} \notin (-\pi, \pi]$  are exponentially suppressed. Therefore, in the limit of infinite  $\lambda$ , the FP determinant (36) can be written as follows:

$$\Delta_{FP}^{-1}[\theta; \lambda] = \int_{-\infty}^{\infty} \mathcal{D}\omega \sum_{k \in \mathbb{Z}(c_1)} \exp\left\{-\lambda \|\theta + d\omega + 2\pi k\|^2\right\}. \quad (37)$$

Using the Hodge–de-Rahm transformation,  $k = \delta\Delta^{-1}dk + d\Delta^{-1}\delta k$ , and making the shift  $\omega \rightarrow \omega - \Delta^{-1}\delta k$  we get

$$\Delta_{FP}^{-1}[\theta; \lambda] = \text{const} \int_{-\infty}^{\infty} \mathcal{D}\omega \sum_{\substack{s \in \mathbb{Z}(c_2) \\ ds=0}} \exp\left\{-\lambda \|\theta + d\omega + 2\pi\delta\Delta^{-1}s\|^2\right\}, \quad (38)$$

where we have changed the variables,  $s = dk$ . The integration over  $\omega$  gives

$$\Delta_{FP}^{-1}[\theta; \lambda] = \text{const} \sum_{\substack{s \in \mathbb{Z}(c_2) \\ ds=0}} \exp\left\{-\lambda \left(d\theta + 2\pi\delta\Delta^{-1}s, \Delta^{-1}(d\theta + 2\pi\delta\Delta^{-1}s)\right)\right\}. \quad (39)$$

To proceed further we separate the gauge field  $\theta$  into regular (photon) and singular (monopole) parts following Ref. [11],

$$\theta = \theta^{phot} + \theta^{mono}, \quad \theta^{mono} = 2\pi\Delta^{-1}\delta p[j], \quad (40)$$

---

<sup>2</sup> Here and in the following we use the we use the differential form notations on the lattice:  $(a, b) = \sum_l a_l b_l$ ,  $\|\theta\|^2 = (\theta, \theta)$ . The operations  $d\theta$  and  $\delta\theta$  are the lattice curl and divergence, respectively. The Laplacian is denoted as  $\Delta = \delta d + d\delta$ .

where the dual one-form  $*j$  represents the monopoles on the dual lattice sites. The one-form on the dual lattice,  $p[j]$ , defines the Dirac lines which connect the monopoles and anti-monopoles,  $\delta^*p[j] = *j$ .

The photon part  $\theta^{phot}$  is free of singularities while the monopole part  $\theta^{mono}$  contains the information about all monopole singularities:

$$\frac{1}{2\pi}d[d\theta^{phot}]_{2\pi} = 0, \quad \frac{1}{2\pi}d[d\theta^{mono}]_{2\pi} = j. \quad (41)$$

Here the DeGrand–Toussaint definition of the monopole [12] has been used. Substituting (40) into (39) we get, after a little algebra,

$$\Delta_{FP}^{-1}[\theta; \lambda] = \text{const} \exp\left\{4\lambda(j, \Delta^{-2}j)\right\} \sum_{\substack{s \in \mathbb{Z}(c_2) \\ ds=0}} \exp\left\{-\lambda S_{gf}(\theta^{phot}, p[j] + s)\right\}, \quad (42)$$

with

$$S_{gf}(\theta^{phot}, p) = \left(d\theta^{phot} + 2\pi p, \Delta^{-1}(d\theta^{phot} + 2\pi(p[j] + s))\right). \quad (43)$$

The meaning of the last equations is the following. The gauge transformation (34) contains both regular ( $d\omega$ ) and singular ( $k$ ) parts. The former transforms the photon part of the gauge field while the latter changes the monopole part shifting the Dirac string (but leaving the monopoles  $j$  intact). We have already integrated out the regular gauge transformations, therefore (42) depends explicitly on  $d\theta^{phot}$  which is invariant under regular gauge transformations,  $\theta^{phot} \rightarrow \theta^{phot} + d\omega$ . The sum in (42) over all possible shifts of the Dirac lines,

$$*p[j] \rightarrow *p[j] + *s, \quad (44)$$

corresponds to the integration over all singular gauge transformations (remember that  $*s$  is the closed line on the dual lattice,  $\delta^*s = 0$ ). Thus (42) is implicitly invariant under the singular gauge transformations as well.

In the limit  $\lambda \rightarrow \infty$  the only contribution to the FP determinant is given by the *global* minimum of the gauge fixing functional (43) with respect to the variations (44) of the Dirac line,

$$S_{gf}^{min}(\theta^{phot}, j) = \min_{ds=0} S_{gf}(\theta^{phot}, p[j] + s). \quad (45)$$

If the photon field is absent, the minimum (45) is given by the Dirac line with minimal ‘‘Coulomb interaction’’ (*c.f.* (43)). For a lattice monopole and anti-monopole separated along one axis this line is the shortest path connecting the pair.

We substitute the FP unity (36,42) into the partition function of compact electrodynamics,

$$Z = \int_{-\pi}^{\pi} \mathcal{D}\theta e^{-S(\theta)}; \quad (46)$$



then we transform the gauge field,  $\theta \rightarrow \theta^{(-\omega)}$  and get the product of the gauge orbit volume,  $\int \mathcal{D}\omega$ , and the partition function within the fixed gauge,

$$Z_{gf} = \int_{-\pi}^{\pi} \mathcal{D}\theta e^{-S(\theta) - \lambda \|\theta\|^2} \Delta_{FP}[\theta; \lambda]. \quad (47)$$

Separating the gauge field on the monopole and photon parts as indicated by (40) and using the Hodge–de-Rahm transformation, one can show that

$$\|\theta\|^2 = (\delta\theta^{phot}, \Delta^{-1}\delta\theta^{phot}) + \left( \theta^{phot} + 2\pi p[j], \Delta^{-1}(\theta^{phot} + 2\pi p[j]) \right) - 4\pi^2(j, \Delta^{-2}j). \quad (48)$$

According to eqs. (42,45,47) the only non–vanishing contribution to the partition function in the limit  $\lambda \rightarrow \infty$  comes from the global minimum (48) in the gauge orbit. Comparison of (45) and (48) shows that this minimum is defined by the following conditions:

$$\delta\theta^{phot} = 0 \quad (49)$$

together with

$$S_{gf}[\theta^{phot}, p[j]] = S_{gf}^{min}(\theta^{phot}, p[j]), \quad (50)$$

where  $S_{gf}$  and  $S_{gf}^{min}$  are given in (43) and (45), respectively.

In the continuum limit the condition (49) leads to the usual Landau gauge condition,

$$\partial_{\mu} A_{\mu}^{phot} = 0, \quad (51)$$

while the condition (50) can be formulated as a requirement for the Dirac lines to form a configuration with as small as possible length:

$$\min_{\delta^* p[j] = \delta j} \text{Length}(p[j]), \quad (52)$$

Indeed, the Dirac lines,  ${}^*p[j] = {}^*p_1[j] + {}^*p_2[j] + \dots$ , correspond to the singular  $\delta$ –functions in the continuum limit. Here  ${}^*p_i$  correspond to mutually unconnected pieces of these lines. The self–interaction of the Dirac lines in (50),  $\sum_i ({}^*p_i[j], \Delta^{-1}{}^*p_i[j])$ , contains the term  $\alpha \sum_i \text{Length}(p_i[j])$  (with a logarithmically divergent coefficient  $\alpha$ ) plus finite terms. The ‘‘Coulomb interaction’’ of different pieces of the Dirac lines,  $({}^*p_i[j], \Delta^{-1}{}^*p_k[j])$ ,  $i \neq k$ , as well as the contribution of the regular fields into the condition (50) are finite in the continuum limit. Thus the only essential contribution to the condition (50) in the continuum limit is given by the term  $\alpha \sum_i \text{Length}(p_i[j]) \equiv \alpha \text{Length}(p[j])$ , which gives the condition (52).

Thus we conclude that in the continuum limit the minimal Landau gauge for the compact gauge fields is reduced to the local gauge condition (51) for the regular fields and a non–local condition (52) – the requirement for the total length of the Dirac lines to be as small as possible – for the singular fields. This result can easily be generalized to the  $4D$  case.

## IV. NUMERICAL ALGORITHMS BEING USED IN THE ANALYSIS

### A. Monte Carlo Updating

The Monte Carlo algorithm in use for this investigation is a mixture of local and global updates. The local Monte Carlo algorithm is based on a 5-hit Metropolis update sweep in an even-odd fashion, alternating with a microcanonical sweep, also in checkerboard mode. Both together are considered as *one* local update. After three local updates the Metropolis step width is eventually tuned to keep an acceptance in the range between 40 % and 60 %.

For better ergodicity, in particular in the presence of an external field (considered in Ref. [6]), also global updates have been included, following the ideas of Ref. [13]. In the equilibrium regime, after every three complete local updates, a global refreshment step is attempted. We try to add one unit of flux to the dynamical gauge field, with random sign in one of the three directions randomly selected. The proposed flux addition is subject to a global Metropolis acceptance check.

For example, one unit of flux in the  $\mu\nu$  plane is introduced with the help of the following gauge field shift [13]  $\theta_{\vec{x},\mu} \rightarrow [\theta_{\vec{x},\mu} + \tilde{\theta}_{\vec{x},\mu}]_{\text{mod } 2\pi}$ :

$$\begin{aligned}\tilde{\theta}_{\vec{x},\nu} &= \frac{\pi}{L_\mu}(2 x_\mu - L_\mu - 1), & \tilde{\theta}_{\vec{x},\nu} &= 0 \text{ for } x_\nu \neq L_\nu, \\ \tilde{\theta}_{\vec{x},\mu} &= \frac{2\pi}{L_\mu} L_\nu (1 - x_\nu), & \tilde{\theta}_{\vec{x},\rho} &= 0, \quad \rho \neq \mu, \nu.\end{aligned}\tag{53}$$

The acceptance rate of the global step changes with  $\beta$  in a different way, depending on the lattice geometry. In our  $T = 0$  studies (on  $32^3$  lattices) we found that the acceptance of global update steps is dropping (more rapidly than exponentially) from 0.48 at  $\beta = 1.0$  to 0.0056 at  $\beta = 2.0$ . For higher  $\beta$  practically no global offers are successful.

In our  $T \neq 0$  studies on  $32^2 \times 8$  lattices, however, we found the acceptance changing smoothly (nearly exponentially, even across the deconfining transition !) from 0.58 at  $\beta = 1.0$  to 0.18 at  $\beta = 3.0$ . A closer look reveals that the higher acceptance rate is due to more frequent global flux changes in the 12 (*i.e.* “magnetic”) direction.

In summary, one total Monte Carlo update cycle consists of three cycles of local update, each consisting of a Metropolis sweep followed by a microcanonical sweep, interchanging with a global update as described above.

In the finite temperature case, the measurement of  $D_T$  turns out to be highly sensitive with respect to the insufficient removal (by the gauge fixing procedure and its repetitions, see the next subsection) of Dirac strings wrapping around the third direction. This is a case where the results with and without global updates, mainly adding and subtracting fluxes through the 12 plane, differ. We comment on this problem and how to deal with it in Section VI.

### B. Landau Gauge Fixing

The Landau gauge has been chosen first of all because it is the most popular gauge to define a gauge field propagator. In this gauge the gauge propagator (5) is expected to fulfill the transversality condition

$$F(q^2) = q_\mu D_{\mu\nu}(\vec{q}) q_\nu \equiv 0.\tag{54}$$

In the case of zero temperature, for example, this allows to describe the propagator by a single function  $D(q^2)$  alone, defined by

$$D_{\mu\nu}(\vec{q}) = \left( \delta_{\mu\nu} - \frac{q_\mu q_\nu}{q^2} \right) D(q^2) . \quad (55)$$

We will see that for any practical implementation of the Landau gauge (54) is slightly violated. This degree of violation can, however, be easily controlled by sharpening the convergence criteria of the gauge-fixing algorithm. More important is the remark that in the case of the *angle*-definition of the vector potential (6) it is really necessary to select the transversal part by projection using (15) and (16). Then it is interesting to see where (*e.g.* in momentum space) the violation of transversality, quantified by the longitudinal propagator  $F$ , is coming from.

There is a second reason to choose the Landau gauge. We intend to split the gauge field into a regular (photon) and a singular (monopole) part by reconstructing the field due to the Dirac plaquettes which, on the other hand, are forming the monopoles. This reconstruction becomes unique in the Landau gauge.

In order to implement the gauge fixing condition (33) we have chosen a mixture of overrelaxation and non-periodic gauge transformations [14], both applied in alternating order.

Iterative overrelaxation has to be practiced in a checkerboard fashion. Starting, say, with the odd sublattice we have first to find for each odd site  $\vec{n}$  a suitable  $\omega_{\vec{n}}$  which maximizes the following function of  $\omega$

$$\mathcal{G}_{\vec{n}}^{loc}(\theta, \omega) = \sum_{\mu} (\cos(\theta_{\vec{n},\mu} - \omega) + \cos(\theta_{\vec{n}-\vec{\mu},\mu} + \omega)) , \quad (56)$$

which represents the part of  $\mathcal{G}$  actually depending on  $\omega_{\vec{n}}$ , and second to perform immediately the updatings of the neighboring link angles

$$\begin{aligned} \theta_{\vec{n},\mu} &\rightarrow \theta_{\vec{n},\mu} - \omega \\ \theta_{\vec{n}-\vec{\mu},\mu} &\rightarrow \theta_{\vec{n}-\vec{\mu},\mu} + \omega . \end{aligned} \quad (57)$$

This can be done simultaneously for half of the sites, namely  $\vec{n} \in \Lambda_{odd}$ . Afterwards the same procedure is applied to the even sublattice. One odd/even pair of gauge updates constitutes one single iterative overrelaxation step. Each overrelaxation iteration is followed by a zero mode subtraction (to be explained in the next subsection).

The angle  $\omega_{\vec{n}}$  can be easily found as

$$\tan(\omega_{\vec{n}}) = \frac{\sum_{\mu} (\sin(\theta_{\vec{n},\mu}) - \sin(\theta_{\vec{n}-\vec{\mu},\mu}))}{\sum_{\mu} (\cos(\theta_{\vec{n},\mu}) + \cos(\theta_{\vec{n}-\vec{\mu},\mu}))} . \quad (58)$$

These gauge angles are multiplied by the overrelaxation factor,  $\omega_{\vec{n}} \rightarrow \eta \omega_{\vec{n}}$  and bounded by  $|\omega_{\vec{n}}| < \pi$  before the iteration (57) is performed on all links. A good overrelaxation parameter has been found to be  $\eta = 1.8$ . According to our experience from studies on  $16^3$  lattices this  $\eta$  leads to fastest convergence, almost independently of  $\beta$ . This value has then been applied for all iterative gauge fixings.

The overrelaxation usually will be stopped if in the last overrelaxation step the average increase of the gauge functional  $\mathcal{F}$  (32) per link was found less than  $10^{-6}$ . After this has

been discovered, the gauge fixing procedure ends with a final zero mode subtraction (see below).

At any *local extremum* of  $\mathcal{F}$  (32) the following condition would be satisfied everywhere on the even *and* odd sublattice:

$$(\partial_\mu A_\mu)_{\vec{n}} \equiv \sum_\mu \left( A_{\vec{n}+\frac{1}{2}\vec{\mu},\mu} - A_{\vec{n}-\frac{1}{2}\vec{\mu},\mu} \right) \equiv \frac{1}{g a} \sum_\mu \left( \sin(\theta_{\vec{n},\mu}) - \sin(\theta_{\vec{n}-\hat{\mu},\mu}) \right) = 0. \quad (59)$$

Having the vector potential localized on the midpoints of links, its divergence is naturally defined on sites  $\vec{n}$ . Exact vanishing of the divergence of  $A_\mu$  can be expected in the result of Landau gauge fixing only for the *sinus*-definition of the vector potential  $A_\mu$ .

The algorithm outlined above will in general not lead to the absolute (global) maximum of the gauge functional  $\mathcal{F}$  (32). Typically it will get stuck in one of the local maxima, which are called Gribov copies of the true maximum. This is the so-called Gribov problem. It is partially cured by repeating the same gauge fixing procedure, applying it to random gauge copies of the original Monte Carlo configuration  $\theta^{MC}$ , assuming that one of these copies might be situated in the basin of attraction of the true maximum. The number of gauge equivalent configurations produced to restart the gauge fixing is denoted as  $N_G$ , and the iterative gauge fixing generically leads to really different maxima. We have then to content with the *best out of all*  $N_G + 1$  *local maxima* of the gauge functional. The convergence, with increasing  $N_G$ , of a gauge dependent quantity evaluated on a given gauge field ensemble with the help of the best Gribov copy gives an indication about the sensitivity of this quantity with respect to the misidentification of the true maximum. We have applied this philosophy to two sets of data, the propagator data itself at large or small momenta, and to the fit parameter emerging from a fit of the gauge boson propagator. One should not be surprised that the number  $N_G$ , which is necessary to achieve uniform convergence of the propagator in momentum space and/or of the fit parameters, differs strongly between zero and finite temperature. At finite temperature there are strong differences between  $D_L$  and  $D_T$ .

In section III we have stressed the importance to find a local maximum of (32) accompanied by a minimal length of Dirac strings. Within our implementation, the start from a new random gauge copy is done in the hope to produce a new Gribov copy reachable from the previous ones only by a discrete gauge transformation. We have monitored the number of Dirac strings in each of the local maxima of the gauge functional  $\mathcal{F}$  (32). Each time the recent best value of the gauge functional was replaced by a better (higher) one, the number  $N_D$  of Dirac strings detected in the correspondingly best Gribov copy was decreasing compared to the previous one.

In Fig. 1 we show scatter plots relating the gauge functional  $\mathcal{F}$  to the number of Dirac strings per direction  $N_i^D$  ( $i = 1, \dots, 3$ ) for two thinned ensembles of 100 out of 1000 equilibrium configurations on  $32^2 \times 8$  lattices, each of them entering with 101 Gribov copies (local maxima of  $\mathcal{F}$ ). Fig. 1 (a) refers to  $\beta = 2.0$  (confined phase) and shows all local maxima (Gribov copies). The isotropy of Dirac strings is clearly visible. Fig. 1 (b) shows how in the deconfined phase the number  $N_3^D$  of temporal Dirac strings is correlated with the locally maximal value of  $\mathcal{F}$ . Fig. 1 (c) shows it for the  $N_1^D$  and  $N_2^D$  (number of spatial Dirac strings). In both cases a slight tendency of clustering near multiples of 8 or 32 (the respective periodicity of the lattice) is visible, in particular for the highest values of  $\mathcal{F}$ . The selection of the best copies restricts the ensemble to bigger  $\mathcal{F}$  and smaller  $N_i^D$  as shown in Fig. 1 (d). In the confinement phase the Dirac strings are still approximately isotropic. In the deconfined phase, however, the highest values of  $\mathcal{F}$  are correlated with low multiplicity

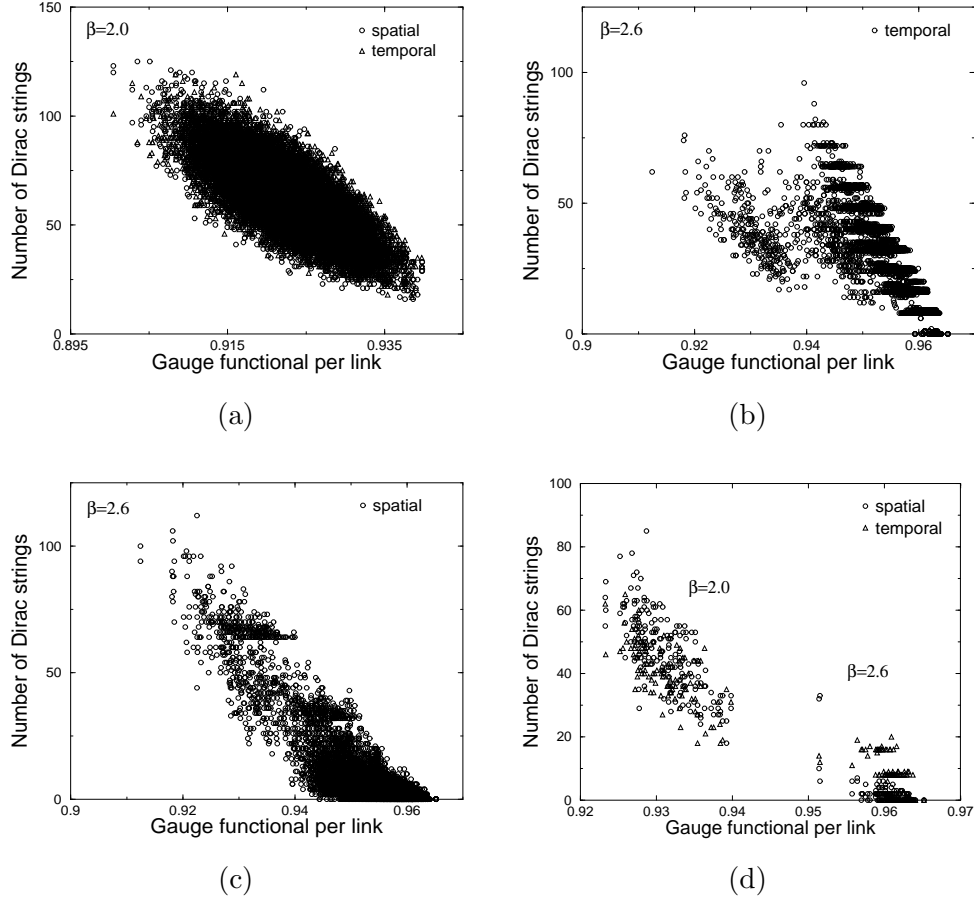


FIG. 1: Scatter plots of the average gauge functional  $\mathcal{F}(\theta)$  per link and the related number for the Dirac strings in the *temporal* ( $N_3^D$ ) and/or the *two spatial* ( $N_1^D$  and  $N_2^D$ ) directions for 100 configurations on a lattice  $32^2 \times 8$ : (a)  $N_3^D$ ,  $N_1^D$  and  $N_2^D$  vs  $\mathcal{F}(\theta)$  in the confinement phase ( $\beta = 2.0$ ), each configuration represented by 101 Gribov copies; (b)  $N_3^D$  vs  $\mathcal{F}(\theta)$  in the deconfinement phase ( $\beta = 2.6$ ); (c) same as in (b) for  $N_1^D$  and  $N_2^D$ ; (d) the two samples represented only by the best out of 101 Gribov copies.

of  $N_1^D$  and  $N_2^D$ , and  $N_3^D$  corresponding to zero, one or a few periodically winding Dirac strings more frequently in the temporal direction.

We stress, that the configurations, the gauge fixing of which has been investigated here in some detail, had been produced with the update algorithm including global updates. Winding Dirac strings of some life time are also produced in ensembles which are generated *without* global updates, however less frequently. Therefore, the inefficiency of the random gauge transformation to explore more of the gauge orbit is an handicap also if global updates are suppressed. We will see later that certain problems which show up in the finite temperature propagator  $D_T$  can be ameliorated, but not completely cured, by abandoning global updates and increasing the number of Gribov copies.

We had not the opportunity to reconstruct exactly the spatial conformation of the Dirac strings in each gauge copy. But for each gauge copy we can determine whether double Dirac strings (running along a certain direction) can be definitely excluded or cannot. At low  $\beta$  this can never be excluded, but at high  $\beta$  this can be used as an additional criterion to reject Gribov copies which contain double Dirac strings.

Although the stopping criterion was formulated for the *global increase* of  $\mathcal{F}$  we did not find a systematic *local variation*, depending on the distance from a monopole, of the violation of (59), expressed by the quantity

$$(\partial_\mu A_\mu)_{\vec{n}}^2 \equiv \left\{ \sum_\mu \left( A_{\vec{n}+\frac{1}{2}\vec{\mu},\mu} - A_{\vec{n}-\frac{1}{2}\vec{\mu},\mu} \right) \right\}^2. \quad (60)$$

This suggests that the differential gauge condition (59) is uniformly approaching zero.

In contrast to this, we found a systematic local variation of the local gauge functional itself,

$$\mathcal{F}_{\vec{n}}^{loc}(\theta) = \sum_\mu (\cos(\theta_{\vec{n},\mu}) + \cos(\theta_{\vec{n}-\vec{\mu},\mu})), \quad (61)$$

with the distance from a monopole. Near to a monopole, the value of it is suppressed compared to the bulk average. This is illustrated in Fig. 2 for  $\beta = 1.0$  and  $\beta = 2.0$ .

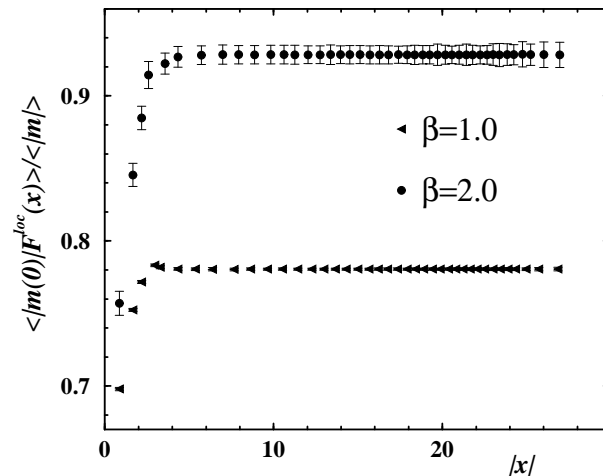


FIG. 2: Suppression of the local gauge functional  $\mathcal{F}_{\vec{n}}^{loc}$  near to a monopole for  $\beta = 1.0$  and  $\beta = 2.0$ . For better presentation part of the data points are not plotted. Notice the  $\beta$  dependence of the bulk average of  $\mathcal{F}_{\vec{n}}^{loc}$ .

### C. Zero Mode Subtraction

There are certain modes of the gauge field which are not suppressed by the action. If they are not taken care of properly, the gauge field propagator is known to be spoiled [14]. For instance, adding some constant to all link angles  $\theta_{\vec{n},\mu}$  in one particular direction does not change the action (1), as well as adding a multiple of  $2\pi$  to one particular link angle. Non-periodic gauge transformations can be considered to implement these changes. We have used it in our simulations to immediately eliminate zero modes related to the appearance of a volume average of the link angles in a given direction

$$\overline{\theta}_\mu = \sum_{\vec{n}} \theta_{\vec{n},\mu} / |\Lambda|, \quad (62)$$

where  $|\Lambda|$  is the lattice volume. We subtract this volume average from each link angle  $\theta_{\vec{n},\mu}$  in  $\mu$  direction,

$$\theta_{\vec{n},\mu} \rightarrow \theta_{\vec{n},\mu} - \overline{\theta}_{\mu} + 2\pi k, \quad (63)$$

with integer  $k$  chosen such that  $\theta_{\vec{n},\mu}^g \in (-\pi, \pi]$ . This operation can be imagined as resulting from a gauge function  $g_{\vec{n}} = -\overline{\theta}_{\mu} n_{\mu}$  (no summation!) which is in general non-periodic. This special sort of gauge fixing is completed when zero modes in all  $d$  directions have been subtracted.

The zero-mode subtraction step is applied after each overrelaxation step. Thus it is always performed before the measurements are done on the gauge-fixed configuration.

In our runs we measured the photon propagator after each 10th total Monte Carlo update cycle to avoid as much as possible autocorrelations. Typically we used 500 gauge-fixed configurations per data point for the  $32^3$  lattice and about 2000 configurations for the  $32^2 \times 8$  lattice.

## V. THE ZERO-TEMPERATURE PROPAGATOR IN LANDAU GAUGE

In coordinate space, the gauge boson propagator that is studied, is read

$$D_{\mu\nu} \left( \vec{m} + \frac{1}{2}\vec{\mu} - \vec{n} - \frac{1}{2}\vec{\nu} \right) = \langle A_{\vec{m}+\frac{1}{2}\vec{\mu},\mu} A_{\vec{n}+\frac{1}{2}\vec{\nu},\nu} \rangle \quad (64)$$

with the *angle*- or *sinus*-definition of  $A$ . For brevity, we will refer to this propagator later in momentum space as  $D_{\mu\nu}^{ang}$  or  $D_{\mu\nu}^{sin}$ . The two scalar functions occurring in momentum space (10) we will denote as  $D^{ang}$  and  $F^{ang}$  or  $D^{sin}$  and  $F^{sin}$ , respectively. The last one,  $F^{sin}$  should vanish in the Landau gauge. We have observed that this is indeed the case with an accuracy determined by the stopping criterion of the iterative overrelaxation. For the *sinus*-propagator the transversal part could be calculated directly just by evaluating and summing the diagonal components appearing in (16). When the longitudinal propagator vanishes only *approximately*, one can extract the transverse propagator following (15, 16).

In Fig. 3 we show the different forms of the transverse propagator  $D^{sin}$  and its components as well as the vanishing longitudinal propagator  $F^{sin}$ . These data have been obtained on a  $32^3$  lattice for (a)  $\beta = 1.0$  and (b)  $\beta = 1.8$ , with  $N_G = 20$  Gribov copies evaluated in addition to each original Monte Carlo configuration. The data at other  $\beta$  have been produced under the same conditions. In Fig. 4 the same is presented for  $D^{ang}$ , its components and non-vanishing  $F^{ang}$ .

For the *angle*-definition of  $A_{\mu}$ , the decomposition into components is strictly additive (31). We have observed that the longitudinal propagator  $F^{ang}$  and its components are well described by a form  $F(p^2) = P p^2$ , where  $P$  is a constant. We find that  $F^{ang,phot}$  practically coincides with the full  $F^{ang}$ . The size of  $F^{ang}$  and its photon component is of the same order of magnitude as the transversal part at  $\beta = 1.0$ , while the monopole and mixed part are one order of magnitude smaller. At  $\beta = 1.8$ , the size of  $F^{ang}$  and its photon component is an order of magnitude smaller than at  $\beta = 1.0$ , while the monopole and mixed part are negligible.

For the *sinus*-definition of  $A_{\mu}$ , the monopole part of the transversal propagator  $D^{sin,mono}$  has a maximum in the low momentum region (which moves with higher  $\beta$  more and more

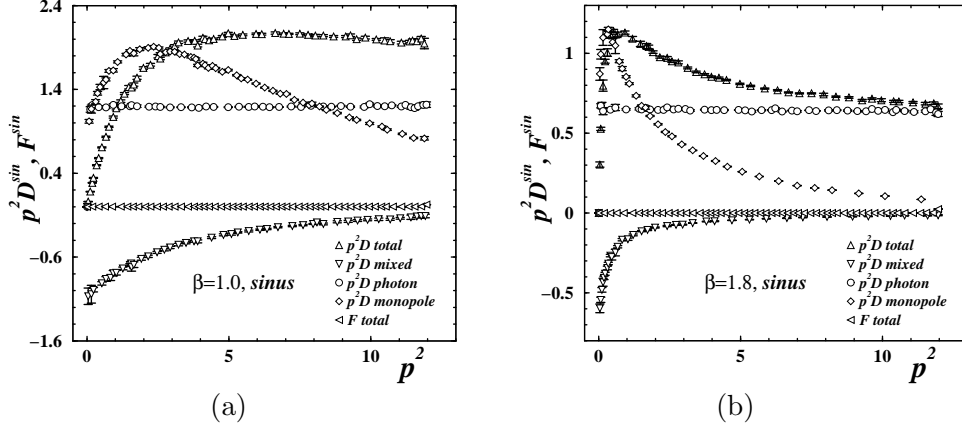


FIG. 3: The Landau gauge *sinus*-propagator as a function of  $p^2$  measured on a  $32^3$  lattice : for the transverse part,  $p^2 D^{sin}$  ((a) at  $\beta = 1.0$  and (b) at  $\beta = 1.8$ ) we show the full propagator, the singular (mono), the regular (phot) and the mixed contribution for comparison. In addition, we show the (vanishing) longitudinal propagator  $F^{sin}$ . The data represent the evaluation of  $N_G = 20$  gauge copies. For better presentation part of the data points are not plotted.

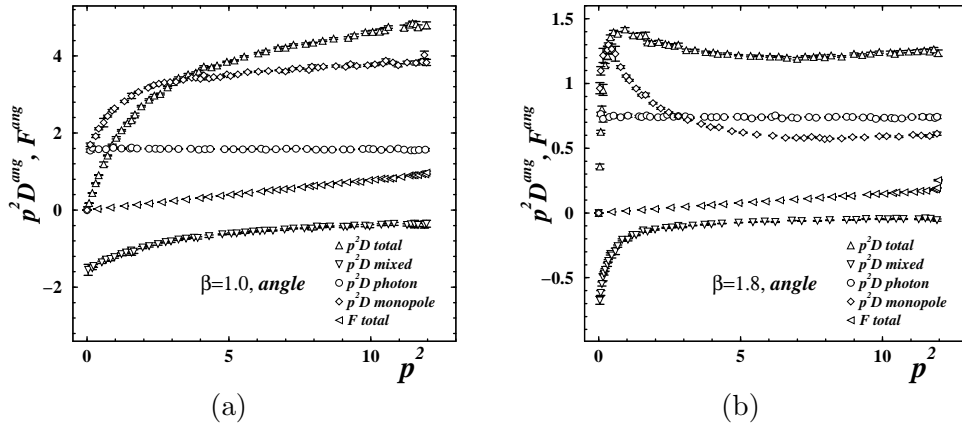


FIG. 4: The same as in Fig. 3 for the Landau gauge *angle* propagator. Notice the nonvanishing longitudinal propagator  $F^{ang}$  decreasing with growing  $\beta$ .

towards  $p^2 = 0$ ) before it drops towards  $p^2 = 0$ . For the *angle*-definition, a maximum of  $D^{ang,mono}$  develops only for  $\beta > 1.0$ .

Summarizing, we have observed that transversal part  $F$  is either zero (for the  $\sin\theta$  definition of the gauge field in the correlator) or it is non-zero, and then it coincides with the photon part (for the  $\theta$  definition). Therefore, at zero temperature the Landau gauge propagator  $D_{\mu\nu}^{ang}$  is not completely transversal. This is entirely due to the difference between the definitions of the vector potential. This discrepancy, expressed by the nonvanishing  $F^{ang}$ , becomes ameliorated at higher  $\beta$ .

For both definitions of  $A_\mu$  we find that the regular (photon) part of the transversal propagator is singular at  $p^2 \rightarrow 0$  like  $D^{phot} \sim 1/p^2$ , while the full transversal propagator is not. Following Ref. [7] we try to describe the two by functions of the form

$$D(p^2) = \frac{Z}{\beta} \frac{m^{2\alpha}}{p^{2(1+\alpha)} + m^{2(1+\alpha)}} + C \quad (65)$$



and

$$D^{phot}(p^2) = \frac{Z^{phot}}{\beta} \frac{1}{p^2} + C^{phot}. \quad (66)$$

The model function (65) is similar to some of the functions discussed in Refs. [15, 16] where the propagator in gluodynamics has been studied. In the case of  $T = 0$  we expect these two curves to differ *at all*  $\beta$  in order to accommodate the (permanent) confinement property of the model.

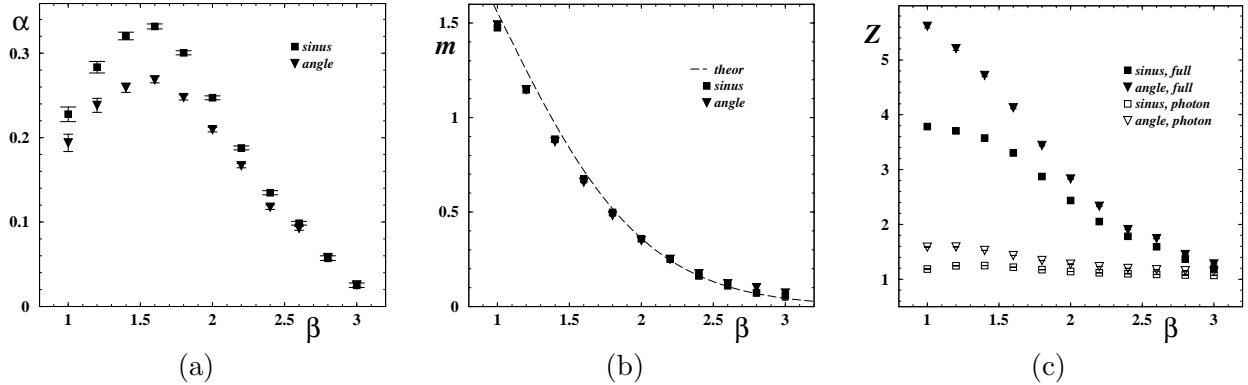


FIG. 5: The best fit parameters for the zero temperature *sinus*- and *angle*-propagators as functions of  $\beta$ : (a) the anomalous dimension  $\alpha$ , (b) the mass parameter  $m$  with the theoretical prediction (67) as dashed line, and (c) the parameters  $Z$  and  $Z_{phot}$  (using (65,66)).

Fig. 5 (a) shows the anomalous dimensions  $\alpha$  first increasing in the low- $\beta$  region. The anomalous dimension for the *angle*- and for the *sinus*-propagator behave quite similar to each other (the dimension for the *angle*-propagator is a bit smaller). As  $\beta$  gets larger than  $\beta \sim 1.5$  the anomalous dimensions start to descent towards zero. This indicates that the anomalous dimension is a function not only of the monopole density which is monotonously decreasing with growing  $\beta$  for all values of the coupling. The (cluster) structure of the monopole configurations may play a significant role for  $\alpha$ .

Fig. 5 (b) shows the mass parameters  $m$  for the *angle*- and the *sinus*-propagator according to (65) as function of  $\beta$ . Both masses are almost equivalent. For the mass there exists a theoretical prediction due to Polyakov [1],

$$m_{th}(\beta) = 2\pi\sqrt{2\beta} \exp\left\{\pi^2\beta_V(\beta) \Delta^{-1}(0)\right\}, \quad (67)$$

where  $\beta_V$  is the Villain coupling constant

$$\beta_V(\beta) = \left[2 \log\left(\frac{I_0(\beta)}{I_1(\beta)}\right)\right]^{-1}. \quad (68)$$

$I_0(\beta)$  and  $I_1(\beta)$  are the modified Bessel functions and  $\beta$  is the Wilson action coupling constant appearing in (1). The prediction (67) is valid for a dilute monopole gas. The agreement between the two data sets and the theoretical curve is very good. The small deviation at lowest  $\beta$  can be attributed to the violation of the dilute gas approximation.

Fig. 5 (c) shows  $Z(\beta)$  and  $Z^{phot}(\beta)$  for the two definitions. We can see, that  $Z$  tends to unity in the limit  $\beta \rightarrow \infty$ , while  $Z^{phot}(\beta) \approx 1$  for all  $\beta$ . The strong deviation of  $Z$  from unity

at small  $\beta$  can be interpreted as a field renormalization by monopoles. Both the monopole density and the deviation of the coupling  $Z$  from unity are descending functions vanishing in the limit  $\beta \rightarrow \infty$ .

The contact terms contained in  $D^{sin}$  and  $D^{ang}$  are not shown here. The photon part of both  $D^{sin}$  and  $D^{ang}$  perfectly vanishes. The full propagator in both cases contains contact terms,  $C^{sin}$  and  $C^{ang}$ , which deviate from zero for smaller  $\beta$ , whereas always  $C^{sin}(\beta) \ll C^{ang}(\beta)$ .

The discussion of Figs. 3 and 4 and of the  $\beta$  dependence of the fit parameters in Fig. 5 was based on the zero-temperature propagators (and its components) obtained throughout with  $N_G = 20$  Gribov gauge copies. The dependence on the number of gauge copies has been investigated carefully for the case of the *angle*-propagator. In the result of this study, the default choice of  $N_G = 20$  for the gauge-fixing procedure at  $T = 0$  has been established.

In Fig. 6 we show different aspects of the approach to the  $N_G \rightarrow \infty$  limit, for  $\beta = 2.0$  as

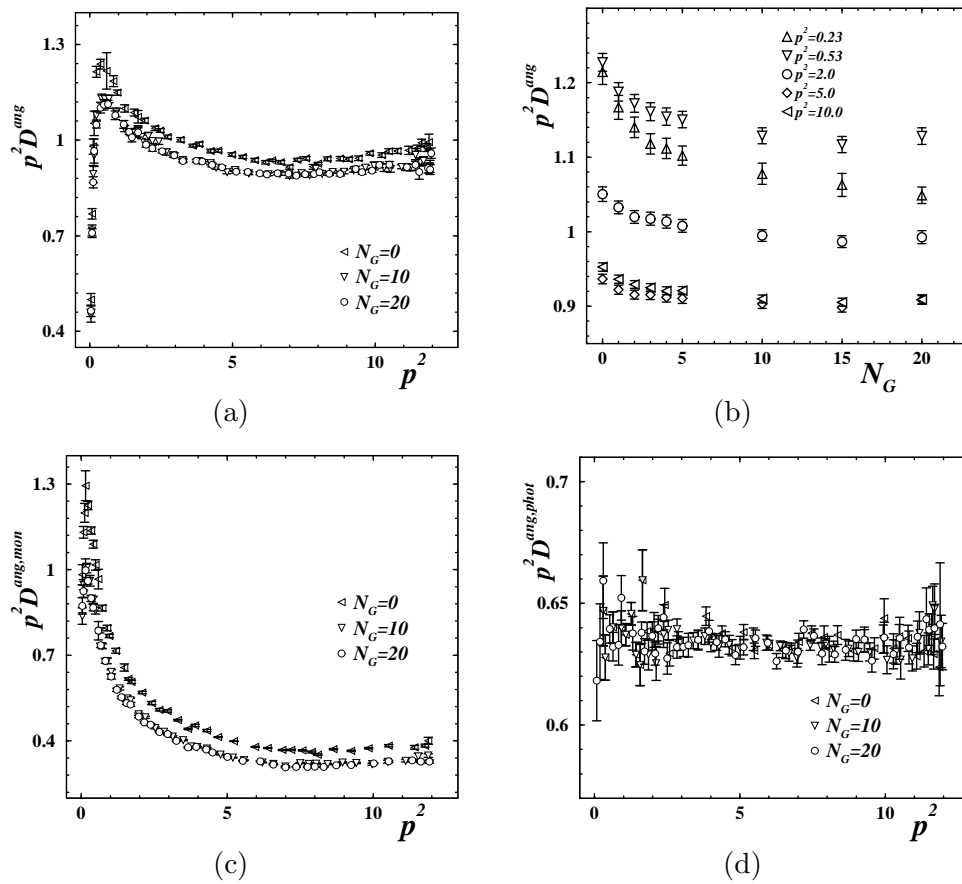


FIG. 6: The dependence of the zero-temperature *angle*-propagator on  $N_G$  for a  $32^3$  lattice (at  $\beta = 2.0$  as an example) : (a) the full transversal propagator for  $N_G = 0, 10, 20$  in the full momentum region; (b) its behaviour as function of  $N_G$  at five selected momenta; (c) the same for the singular (mono) part of the transversal propagator; (d) the same for the regular (phot) contribution to the transversal propagator. Again for better presentation part of the data points are not plotted.

an example. Fig. 6 (a) demonstrates that the transversal propagator evaluated with 10 or 20 gauge copies does not differ essentially, but that the naive evaluation (with  $N_G = 0$ ) would clearly overestimate the propagator all over the momentum range. Fig. 6 (b) shows this

more in detail for five selected momenta. It becomes clear that the dependence is strongest in the region of small momenta, in particular the region *below* the peak. The dependence is strong for the singular part presented in Fig. 6 (c). Again, there is almost no change between  $N_G = 10$  and 20. As can be seen from Fig. 6 (d), there is practically no  $N_G$  dependence in the photon part of the transversal propagator.

We present the resulting dependence of the fit parameters on  $N_G$  in Fig. 7, again for

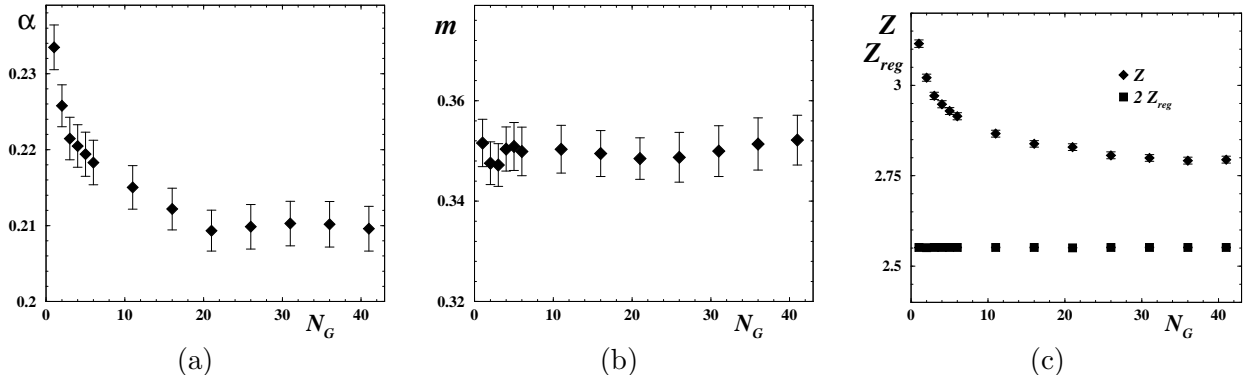


FIG. 7: The best fit parameters for  $D^{ang}$  at zero temperature as a function of  $N_G$  (for  $\beta = 2.0$  as an example): (a) anomalous dimension  $\alpha$ , (b) mass parameter  $m$  and (c) renormalization constants  $Z$  for  $D^{ang}$  and  $D^{ang,phot}$ .

$\beta = 2.0$ . The anomalous dimension  $\alpha$  shown in Fig. 7 (a) drops within 10 % which indicates that the anomalous dimension is sensitive with respect to the minimization of the Dirac strings which is achieved by better and better Gribov copies. The mass presented in Fig. 7 (b) does not change with  $N_G$  which confirms that it is mainly determined by the monopole mass (*i.e.* density).<sup>3</sup> Fig. 7 (c) shows  $Z$  for the full transversal propagator and  $Z^{phot}$  for the photon part. It is not surprising that the parameter associated with the photon part do not change. The parameter describing the full transversal propagator decreases, again by  $\approx 10\%$  within  $N_G < 20$ . One can also observe a slight dependence of  $Z$  on  $N_G$  for  $N_G > 20$ . However, the dependence is indeed very small (about 1%) and not essential for our qualitative discussion.

From the comparison of the *sinus*-propagator and the *angle*-propagator at zero temperature we conclude that the fits of the transversal part give more or less the same parameters, with a  $\beta$  dependence (if appropriate) which is in accordance with the monopole density. Strict transversality itself is guaranteed only in the case of the *sinus*-propagator. In the case of the *angle*-definition an appropriate transversal part has to be extracted by projection (15,16).

## VI. THE FINITE-TEMPERATURE PROPAGATOR IN LANDAU GAUGE

In this Section we report our investigation of the properties of the gauge boson propagator at finite temperatures. With respect to the distinguished direction  $\mu = 3$ , the propagator  $D$  can be separated into transversal and longitudinal components (see Section II for the definitions) denoted as  $D_T$  and  $D_L$ , respectively. We are working on the lattice  $32^2 \times 8$ , in

<sup>3</sup> Let us remind that the monopole positions in a given configuration are gauge independent.

line with Ref. [7], where only the  $D_L$  component of the *angle*-type propagator (with  $p_3 = 0$ ,  $N_G = 20$  and a limited statistics of 500 measurements) has been studied.

The transverse component of the propagator,  $D_T$ , describes the spatial degrees of freedom while the longitudinal component,  $D_L$ , contains gauge fields in Landau gauge both in temporal and spatial directions. The finite temperature propagator data are analyzed again for  $p_3 = 0$ , as a function of  $\mathbf{p}^2$ . In that case  $D_L$  is constructed only from temporal degrees of freedom which, in particular, are responsible for the confinement phenomena. We have fitted the data for both components of the propagator using the fit function (65) invented first in Ref. [7] to describe  $D_{33}$ .

First we have repeated the investigation of the Gribov copy dependence of the propagator components  $D_L$  and  $D_T$ , this time for the *sinus*-definition of the propagator, similar to that conducted for the zero-temperature case with the *angle*-definition. The results are summarized in Fig. 8 at  $\beta$  values near below and above the phase transition. After a few Gribov copy attempts the longitudinal component is almost insensitive to the number  $N_G$ . This can be seen from the left panel of Fig. 8. The fitting parameters  $\alpha_L$ ,  $m_L$ ,  $Z_L$  and  $C_L$  (the latter is not shown here) are rapidly converging and become almost independent of  $N_G$  for  $N_G \gtrsim 7$ . The results at large number of Gribov copies are not sensitive to the fact whether we have suppressed global updates (we made only local updates, see the label “local ”) or not.

The transverse component, however, is strongly dependent on the number of Gribov copies as it can be seen from Fig. 8. All fit parameters  $\alpha_T$ ,  $m_T$  and  $Z_T$  are descending functions of the number of Gribov copies  $N_G$  with included global updates. At  $N_G = 100$  the plateau is not yet reached. Moreover, the results are sensitive whether global updates are included or not, in particular at high values of  $\beta$ . The measurements with only local updates lead to significantly lower fit results. In the deconfinement we would expect vanishing  $m_T$  and  $\alpha_T$ , and  $Z_T \rightarrow 1$ .

The reason for that behavior might be explained as follows: On one side, the “best” gauge functional is realized in *gauge-fixed* configurations without Dirac lines wrapping around the lattice (dominantly in the short temporal direction). Such Dirac lines are continuously created and destroyed by the Monte Carlo process, even if global updates are *not* attempted. The level of “noise” due to wrapping Dirac lines is higher if global updates are included in the Monte Carlo process, which in general would improve the ergodicity of the system, but it represents a problem also if only local updates are used. The presence of wrapping Dirac strings mimics a finite  $\beta$ -independent *lattice* mass  $m_T$  at larger  $\beta$ , the value of which decreases only with increasing temporal extent  $L_T$ . So in the limit of vanishing lattice spacing the dimensionful mass would diverge.

This “Dirac noise” represents a serious challenge for the gauge fixing algorithm. The deterministic part (overrelaxing steepest descent method) described in Section IV B cannot remove it. *Unbiased* random gauge transformations applied to get new start configurations for the deterministic search for further Gribov copies are obviously not effective enough to reduce the “Dirac noise”. A simulated annealing Monte Carlo series of random gauge transformations with the total length of Dirac strings as “gauge action” [17] seems to be more appropriate to select new start configurations for the final steepest descent search.

Having these difficulties in mind, we decided to use in the final measurements at finite temperature, for  $\beta = 2.0$  and larger, only local updates before gauge fixing and to perform  $N_G = 100$  Gribov copy attempts. For both *sinus*- and *angle*-propagator measurements deep in the confinement phase (below  $\beta = 2.0$ ) we used  $N_G = 20$  and global updates where the

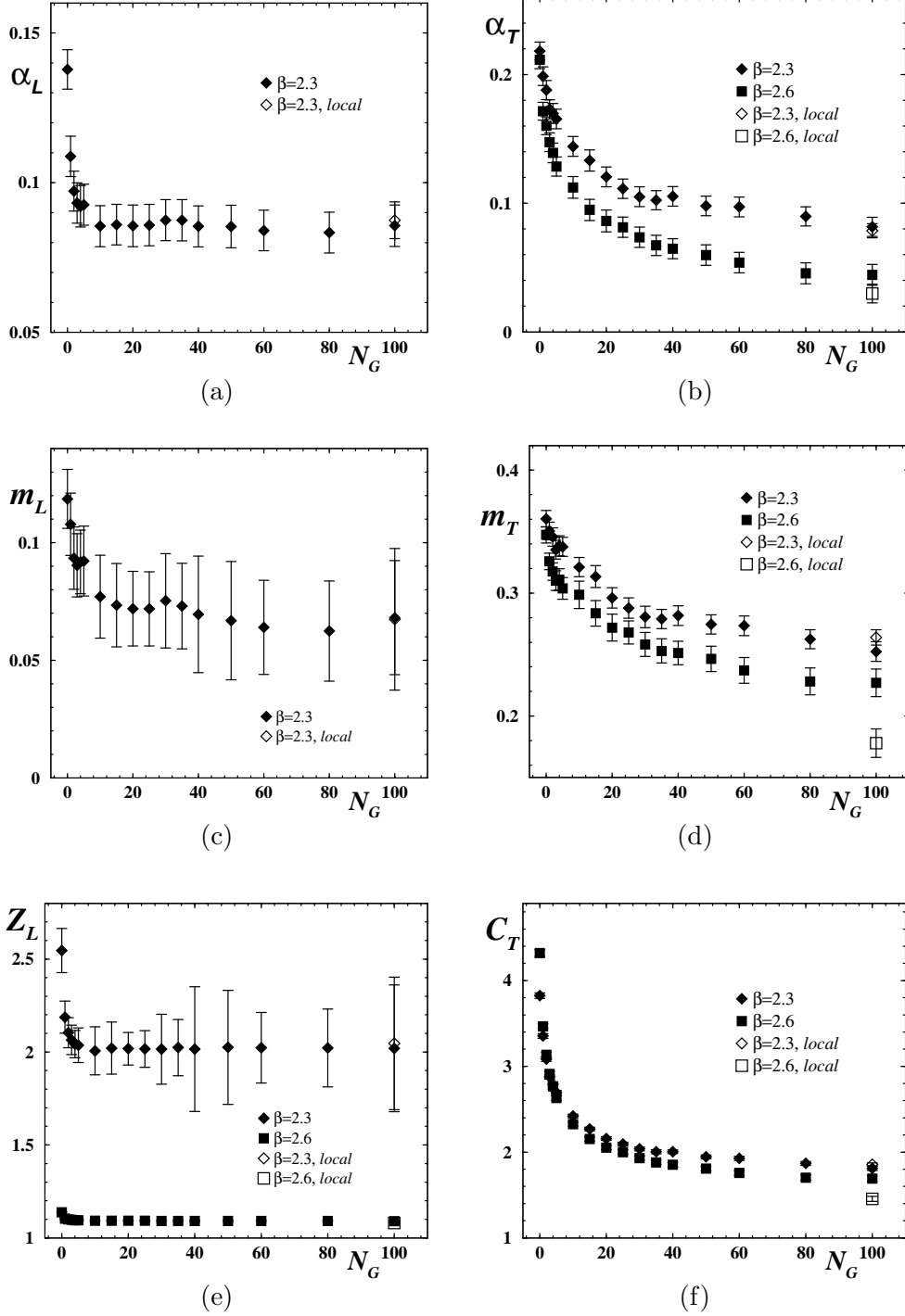


FIG. 8: The Gribov copy dependence of the best fit parameters for the  $D_L$  and  $D_T$  propagators: the anomalous dimension  $\alpha$  (a,b), the mass parameter  $m$  (c,d) and the parameters  $Z$  (e,f). The label “local” corresponds to measurements in Monte Carlo cycles without global updates and with  $N_G = 100$  extra Gribov copies.

results of the zero temperature analysis for the Gribov copy dependence is applicable and the fit parameters of both  $D_L$  and  $D_T$  have to agree within accuracy and should be similar to those for the  $T = 0$  transverse propagator  $D$ . Nevertheless, we have to admit that the

results for the transverse propagator  $D_T$  should be understood only qualitatively.

The results for best fit parameters for  $D_L$  and  $D_T$  are presented in Fig. 9. Let us begin

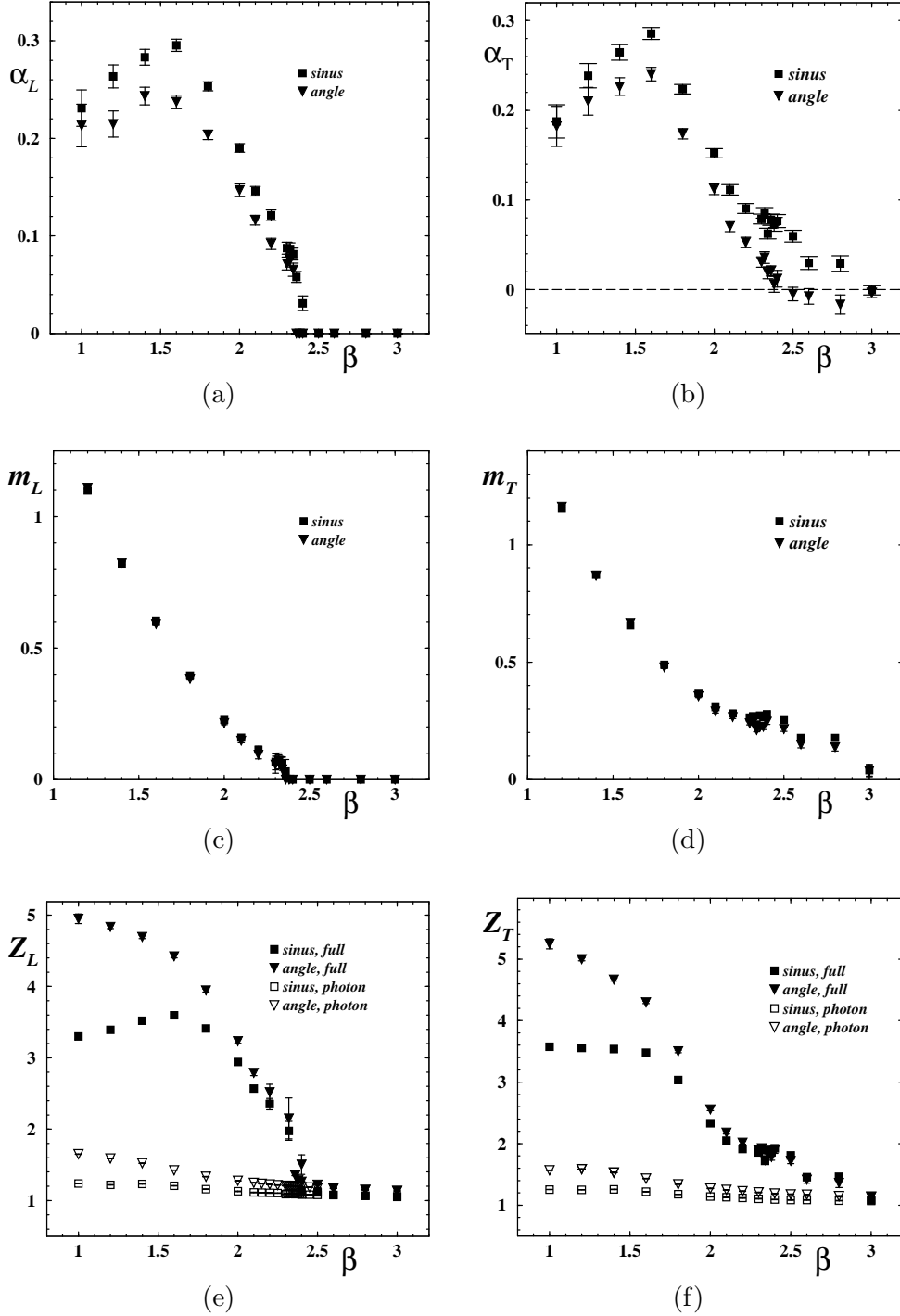


FIG. 9: The best fit parameters for the non-zero temperature *sinus*- and *angle*-propagators as functions of  $\beta$ : the anomalous dimension  $\alpha$  (a,b), the mass parameter  $m$  (c,d), the parameters  $Z$  and  $Z_{phot}$  (e,f). The left column corresponds to  $D_L$ , the right to  $D_T$ . The fits of full propagators are done with the help of (65), the photon contribution is fitted by (66).

with  $D_L$ . At the critical point both the anomalous dimension  $\alpha_L$  and the mass  $m_L$  vanish

while the renormalization parameter  $Z_L$  meets the corresponding parameter for the perturbative photon,  $Z_L^{phot}$ . This behaviour is characteristic both for *angle* and *sinus* types of the propagator and extends our results in Ref. [7]. Note that also here the mass parameters for *sinus*- and *angle*-propagators coincide with each other. However, the anomalous dimensions for these cases slightly differ from each other while the renormalization parameters are significantly different, and the renormalization factor for the *angle*-propagator is bigger than that for the *sinus*-propagator. The latter is expected because  $|\sin \theta| \leq |\theta|$ .

The corresponding quantities for  $D_T$  behave differently for the *angle*- and *sinus*-definitions of  $A_\mu$ , with the remarkable exception of the mass parameter. For example, the anomalous dimension  $\alpha_T$  for the *angle*-propagator vanishes in the vicinity of the critical point and beyond, while the same quantity for the *sinus*-propagator does not vanish. We explain this behaviour as due to insufficient gauge fixing as it can also be guessed from our previous analysis. The same reason explains the fact that the masses  $m_T$  for both definitions of the photon propagators – being remarkably similar – are not vanishing at the critical point. Finally, for both definitions of the propagators the renormalization constants  $Z_T$  do not approach the corresponding  $Z_T^{phot}$  at the critical point. In order to get a reliable behaviour of  $D_T$  part of the propagator one should drastically increase the number of Gribov copies used in the gauge fixing. For the time being this is beyond our computing capabilities. The situation could be improved using a variant of the mentioned simulated annealing Monte Carlo series of random gauge transformations in order to choose more appropriate initial gauge transformed configurations before fixing the gauge.

## VII. CONCLUSIONS

We have studied the gauge boson propagator in cQED<sub>3</sub> both at zero and non-zero temperatures. We have found that the propagators in all cases under investigation can be fitted by (65) which is a sum of the massive propagator with an anomalous dimension plus a contact term. Similarly to the case of  $D_L$  at finite-temperature [7], a nonvanishing anomalous dimension  $\alpha$  is found at  $T = 0$ , too. Moreover, the fact of existence of the anomalous dimension is not associated with a particular type of the gauge boson propagator. We have studied *angle*- and *sinus*-types of the propagators and the corresponding anomalous dimensions are nonvanishing and have a similar behaviour as functions of  $\beta$ .

The existence of the anomalous dimension depends on the presence of the monopole plasma, but it is not directly proportional to the monopole density below  $\beta = 1.5$ . In the confinement phase the monopole plasma is present at any coupling of the system and the density of monopoles is a monotonously decreasing function of the lattice coupling  $\beta$ . A similar behaviour is observed for the anomalous dimension in the case of the  $D_L$  and  $D_T$  propagators. The dimension  $\alpha_L$  extracted from  $D_L$  component of the propagator is vanishing in the vicinity of the phase transition for both definitions (*angle* and *sinus*) of the propagator. However, this does not happen for the *sinus*-definition of the  $D_T$  propagator. We associate this result with insufficient number of the Gribov copies used in the gauge fixing. The  $D_T$  propagator requires much more Gribov copies for the gauge fixing than the  $D_L$  propagator.

Concerning the other parameters of the fits, the mass extracted from the propagator at zero temperature and from the  $D_L$  propagator at non-zero temperature does not depend on the definition of the propagator. The mass for  $T = 0$  case is perfectly described by the Polyakov formula. The  $m_L$  mass is vanishing at the phase transition point as was expected from the disappearance of the monopole plasma at the critical temperature. Beyond the

phase transition point, the  $m_T$  mass measured in this paper does not behave in a physical way due to the severe Gribov copy problem.

### Acknowledgements

M. N. Ch. is supported by the JSPS Fellowship P01023. E.-M. I. gratefully appreciates the support by the Ministry of Education, Culture and Science of Japan (Monbu-Kagakusho) and the hospitality extended to him by H. Toki at the RCNP of Osaka University.

- 
- [1] A. M. Polyakov, Nucl. Phys. **B 120**, 429 (1977).
  - [2] H. R. Fiebig and R. M. Woloshyn, Phys. Rev. **D 42**, 3520 (1990).
  - [3] Y. Hosotani, Phys. Lett. **B 69**, 499 (1977); V. K. Onemli, M. Tas and B. Tekin, JHEP **0108**, 046 (2001).
  - [4] G. Baskaran and P. W. Anderson, Phys. Rev. **B 37**, 580 (1998); L. B. Ioffe and A. I. Larkin, *ibid.* **B 39**, 8988 (1989); P. A. Lee, Phys. Rev. Lett. **63**, 680 (1989); T. R. Morris, Phys. Rev. **D 53**, 7250 (1996).
  - [5] M. N. Chernodub, E.-M. Ilgenfritz and A. Schiller, Phys. Rev. **D 64**, 054507 (2001).
  - [6] M. N. Chernodub, E.-M. Ilgenfritz and A. Schiller, Phys. Rev. **D 64**, 114502 (2001).
  - [7] M. N. Chernodub, E.-M. Ilgenfritz and A. Schiller, Phys. Rev. Lett. **88**, 231601 (2002).
  - [8] H. Kleinert, F. S. Nogueira and A. Sudbø Phys. Rev. Lett. **88**, 232001 (2002); A. Sudbø *et al.*, “Criticality in the 2+1-dimensional compact Higgs model and fractionalized insulators”, cond-mat/0207501.
  - [9] M. N. Chernodub, E.-M. Ilgenfritz and A. Schiller, “String Breaking and Monopoles: a Case Study in the 3D Abelian Higgs Model”, hep-lat/0207020.
  - [10] M. I. Polikarpov, Ken Yee, and M. A. Zubkov, Phys. Rev. **D 48**, 3377 (1993).
  - [11] R. J. Wensley and J. D. Stack, Phys. Rev. Lett. **63**, 1764 (1989).
  - [12] T. DeGrand and D. Toussaint, Phys. Rev. **D 22**, 2478 (1980).
  - [13] P. H. Damgaard and U. M. Heller, Nucl. Phys. **B 309**, 625 (1988).
  - [14] V. K. Mitrjushkin, Phys. Lett. **B 390**, 293 (1997); I. L. Bogolubsky, V. K. Mitrjushkin, M. Müller-Preussker and P. Peter, Phys. Lett. **B 458**, 102 (1999).
  - [15] P. Marenzoni, G. Martinelli, N. Stella and M. Testa, Phys. Lett. **B 318**, 511 (1993); P. Marenzoni, G. Martinelli and N. Stella, Nucl. Phys. **B 455**, 339 (1995); D. B. Leinweber, J. I. Skullerud, A. G. Williams and C. Parrinello, Phys. Rev. **D 60**, 094507 (1999) [Erratum-*ibid.* **D 61**, 079901 (1999)]; A. G. Williams, *Proc. of 3rd Int. Conf. in Quark Confinement and Hadron Spectrum*, hep-ph/9809201.
  - [16] J. P. Ma, Mod. Phys. Lett. **A 15**, 229 (2000).
  - [17] W. Kerler, C. Rebbi and A. Weber, Phys. Lett. **B 348**, 565 (1995).